Journal of Alloys and Compounds 840 (2020) 155747

Contents lists available at ScienceDirect

Journal of Alloys and Compounds

journal homepage: http://www.elsevier.com/locate/jalcom

Interaction of graphene oxide with barium titanate in composite: XPS and DFT studies

D.W. Boukhvalov [a, b, *], I.S. Zhidkov [b], A.I. Kukharenko [b], S.O. Cholakh [b], J.L. Menéndez [c], L. Fernández-García [c], E.Z. Kurmaev [b, d]

[a] College of Science, Institute of Materials Physics and Chemistry, Nanjing Forestry University, Nanjing, 210037, PR China
[b] Institute of Physics and Technology, Ural Federal University, Yekaterinburg, 620002, Russia
[c] Centro de Investigación en Nanomateriales y Nanotecnología, Consejo Superior de Investigaciones Científicas (CSIC)—Universidad de Oviedo (UO)—Principado de Asturias, Avenida de La Vega 4-6 El Entrego, San, Martin Del Rey Aurelio, Asturias, 33940, Spain
[d] M.N. Mikheev Institute of Metal Physics, Russian Academy of Sciences, Ural Branch, Yekaterinburg, 620108, Russia

ARTICLE INFO

Article history:
Received 7 April 2020
Received in revised form
4 May 2020
Accepted 20 May 2020
Available online 24 May 2020

ABSTRACT

By using X-ray photoelectron spectroscopy and density functional theory based calculations, it has been found that graphene in $BaTiO_3$/graphene oxide composites prepared by inexpensive traditional ceramic processing behaves as an active filler. It also induces an interfacial bonding with the formation of Ti—O—C chemical bonds that lead to a reduction of the band gap from 3.4 to 2.4 eV, which is attractive for various photocatalytic applications. The pathway and energetics of hydrogen evolution reaction in acidic and alkaline media over $BaTiO_3$/graphene oxide substrates were checked.

1. Introduction

Monolithic ceramics attract attention due to their intrinsic properties such as high stiffness, strength and stability at high temperatures. However, the presence of impurities, pores and cracks make pure ceramics extremely brittle with poor thermal and electrical conductivity, which significantly limits their practical applications [1]. To solve these problems, ceramic matrix composites have been developed in which an increase in their strength, as well as their thermal and electrical characteristics, was achieved by introducing a secondary reinforcement phase. Recently, nanomaterials with different morphologies and properties, in particular single-walled carbon nanotubes (SWNT) have been used to reinforce monolithic ceramics [2,3]. Improvements of ~100% in fracture toughness and ~20% in flexural strength have been found with the addition of only 1 wt-% SWNTs [4] and an increase of 13 orders of magnitude in the electrical conductivity with 5.7 vol.-% SWNTs [5]. Graphene, the two-dimensional counterpart of carbon nanotubes is also found to be an excellent potential nanofiller in composite materials [6]. The 2D structure of graphene is especially suitable for its use in ceramic composites where processing techniques often employ high pressures. The main advantage of using graphene compared to SWNTs is a higher specific surface area [7] and less tendency to tangle, which makes it easier to disperse into a matrix [8]. Recent works report the formation of stable $BaTiO_3$/graphene composites with enhanced dielectric permittivity [9] and X-ray shielding properties [10]. However, until now, it is not clear whether graphene is a passive or an active filler, or in other words, whether it interacts with a ceramic matrix forming chemical bonds [11]. This interface chemistry and matrix/nanostructures bonding characteristics are complicated subjects that require fundamental understanding at the atomic and electronic level. In connection with this, we have performed a study of the electronic structure of $BaTiO_3$/graphene oxide composite with the help of measurements of X-ray photoelectron spectroscopy (core levels and valence bands) and density functional theory calculations.

2. Experimental and calculation details

$BaTiO_3$/graphene oxide powders with graphene concentration of 1.5% (vol) were prepared as follows: $BaTiO_3$ (Inframat, >99.95% purity) powders for ceramic matrices with an average particle size of around 700 nm were dispersed in distilled water then mixed with the graphene oxide dispersion and, finally, ball milled for 1 h. The homogeneous mixtures were spray dried and uniaxially

* Corresponding author. College of Science, Institute of Materials Physics and Chemistry, Nanjing Forestry University, Nanjing, 210037, PR China.
E-mail address: danil@njfu.edu.cn (D.W. Boukhvalov).

https://doi.org/10.1016/j.jallcom.2020.155747
0925-8388/

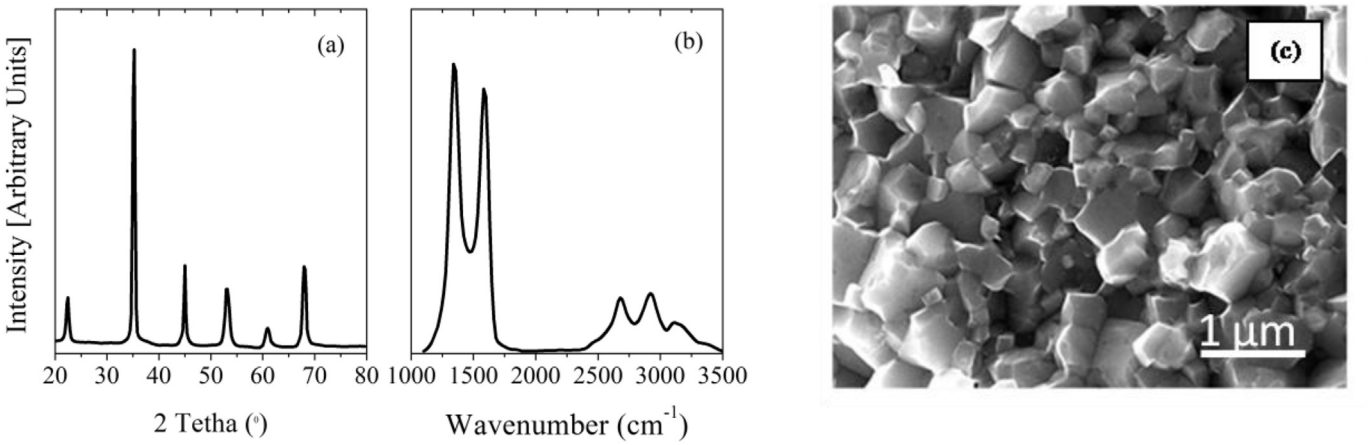

Fig. 1. XRD (a), Raman spectra (b) and FESEM image (c) of $BaTiO_3$/graphene.

pressed (30 MPa) prior to spark plasma sintering in an FCT-HP D25/1 apparatus with a heating rate of 50 °C·min^{-1} under an applied pressure of 80 MPa, a holding time of 1 min and in vacuum (10^{-1} mbar). The final sintering temperature was 1100 °C and densities were close to 100% for $BaTiO_3$/graphene oxide composite.

X-ray photoelectron spectra (XPS) were measured using a PHI 5000 Versa Probe XPS spectrometer (ULVAC Physical Electronics, USA) based on a classic X-ray optics scheme with a hemispherical quartz monochromator and an energy analyzer working in the range of binding energies from 0 to 1500 eV. Electrostatic focusing and magnetic screening was used to achieve an energy resolution of $\Delta E \leq 0.5$ eV for the Al K_α radiation (1486.6 eV). An ion pump was used to maintain the analytical chamber at 10^{-7} Pa, and dual channel neutralization was used to compensate the local surface charge generated during the measurements. The XPS spectra were recorded using Al K_α x-ray emission - spot size was 200 µm, the X-ray power delivered to the sample was less than 50 W, and typical signal-to-noise ratios were greater than 10,000:3.

Powder X-ray diffraction analysis (D8 Advance, BRUKER) were used to determine possible high-temperature chemical reactions between components in sintered samples. Raman spectroscopy was performed on a Renishaw 2000 Confocal Raman Microprobe (Rhenishaw Instruments, England) using a 514.5-nm argon ion laser. Spectra were recorded from 1100 to 3500 cm^{-1}. The microstructure was characterized by field emission scanning electron microscopy (FESEM) in secondary electron mode on a QUANTA FEG 650 using an acceleration voltage of 20 kV.

We used density functional theory (DFT) implemented in the pseudopotential code SIESTA [12], as in our previous studies of similar graphene oxide systems [13,14]. All calculations were performed using the generalized gradient approximation (GGA-PBE) with spin-polarization [15] and implementation of the correction of van der Waals forces [16]. During the optimization, the ion cores were described by norm-conserving non-relativistic pseudopotentials [17] with cut off radii 5.08, 2.42, 1.25, 1.14 and 1.25 a.u. for Ba, Ti, C, O and H respectively, and the wave functions were expanded with localized orbitals and a double-Ж plus polarization basis set for other species. The atomic positions were fully optimized and optimization of the force and total energy was performed with an accuracy of 0.04 eV/Å and 1 meV, respectively. All calculations were carried out with an energy mesh cut-off of 300 Ry and a *k*-point mesh of $8 \times 6 \times 4$ in the Monkhorst-Pack scheme [18].

The X-ray diffraction analysis (Fig. 1a) shows the diffraction peaks corresponding only to the tetragonal phase of $BaTiO_3$. Other phases such as TiC have not been detected and, therefore, they should be below the detection limit of 1% vol. In order to study the structure of the graphene after sintering, Raman spectra were taken (Fig. 1b). Bands D (1355 cm^{-1}) and G (1583 cm^{-1}) are found to be

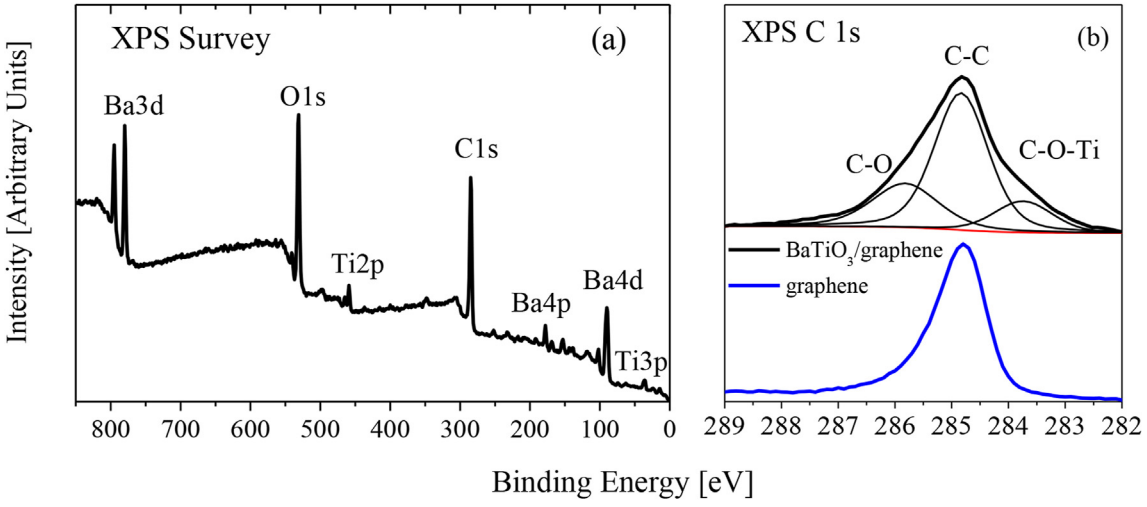

Fig. 2. XPS survey (a) and C 1s (b) spectra of $BaTiO_3$/graphene composite. XPS C 1s of graphene is taken from Ref. [24].

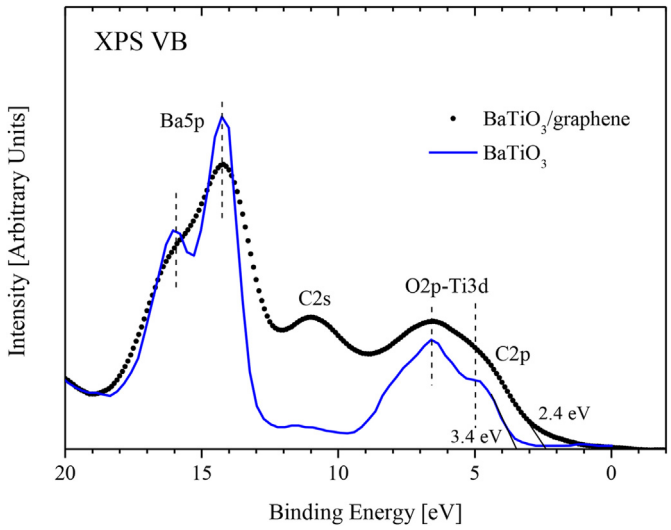

Fig. 3. XPS valence bands of $BaTiO_3$/graphene composite and $BaTiO_3$ [25].

narrow and have similar intensities, with band D being even more intense than band G (ID/IG = 1.06). This ratio is much higher than that of unreduced graphene oxide (ID/IG = 0.91 [19]) and evidences restoration of the graphene structure and conversion of carbon atoms from sp^3 to sp^2. According to Botas et al. [19], the relative intensities of the D, G, and 2D bands indicate that the state of the graphene in these composites is very similar to graphene treated at 1000 °C. The 2D peak is centered around 2690 cm^{-1} and presents a single component which, according to Ferrari et al. [20], implies that the predominant number of stacked layers is one. The field emission scanning electron microscopy image of $BaTiO_3$/graphene oxide composites (Fig. 1c) shows the grain size is around 0.5 μm.

3. Results and discussions

The XPS survey spectrum of $BaTiO_3$/graphene composite is shown in Fig. 2a. One can see that it only contains Ba 3d, O 1s, Ti 2p, C 1s, Ba 4p, Ba 4d and Ti 3p peaks, indicating the presence of Ba, C, Ti and O elements without any other detectable impurities. Fig. 2b shows the XPS C 1s spectrum which is found different with respect to that of graphene oxide and reduced graphene oxide [22]. In addition to two peaks centered at 285.8 and 284.7 eV which can be attributed to C-O and C-C bonds a new peak at 283.7 eV has appeared which can be related to Ti-O-C bonds [19,20]. The ratio of C-O/C-C peaks of XPS C 1s spectrum measured for $BaTiO_3$/graphene (~0.32) is found to be close to that of rGO (~0.25) and much less than in GO (~0.96) [22] which means that the used sample preparation procedure provides the formation of reduced graphene in composite. The presence of Ti-O-C bonds strongly suggests the existence of covalent bonds between $BaTiO_3$ and graphene [19]. The formation of such bonds can be quite important for efficient transport of charge carriers through the composite upon the light excitation to enhance its photocatalytic activity [21]. The hybrid interactions between C 2p and Ti 3d-states is clearly seen from comparison of XPS valence band spectra of $BaTiO_3$/graphene composite and $BaTiO_3$ [23](see Fig. 3). The comparison of these spectra shows that XPS VB of composite is characterized by appearance of additional subband at ~11.0 eV which is due to C 2s-states and broadening of near the Fermi region at the expense of formation of O 2p-Ti 3d-C 2p hybridized states. The valence band offset determined by the linear extrapolation of the leading edge of the XPS VB spectrum with the base line (Fig. 3) shows that it is shifted from 3.4 eV for unmodified $BaTiO_3$ to 2.4 eV for $BaTiO_3$/graphene composite which indicates for band gap reduction in composite. The similar effect is observed in TiO_2/graphene composite [25] where it is found that graphene is hybridized with TiO_2 matrix reducing the band gap and enhancing the photocatalytic activity. In order to reveal the atomic structure of the $BaTiO_3$/graphene interface, DFT-based modeling was performed. The first step is the choice of the proper model. Taking into account the tetragonal symmetry of the $BaTiO_3$ substrate, we have preferred to use a rectangular lattice for graphene. Due to the minimal mismatch between the *c* lattice parameter of $BaTiO_3$ with the lattice parameter of graphene along the armchair direction (4.23 and 4.26 Å respectively), we considered the adsorption of graphene on the (100) surface of $BaTiO_3$. Along another direction three *b* lattice parameters of $BaTiO_3$ almost coincide with five lattice parameters of graphene along zigzag direction (12.09 and 12.31 Å respectively). Note that in contrast to the case of pure graphene on metals, an exact matching between the lattice parameters of graphene and substrate is not required due to the inexactness of the lattice parameter of graphene oxide caused by oxidation [11]. Thus, the supercell for the modeling of $BaTiO_3$/graphene interface can be rather minimalistic (Fig. 4a). This structure can be presented as the line of hexagonal carbon rings along zigzag direction over substrate of four by four unit cells of $BaTiO_3$. Multiplication of the supercell

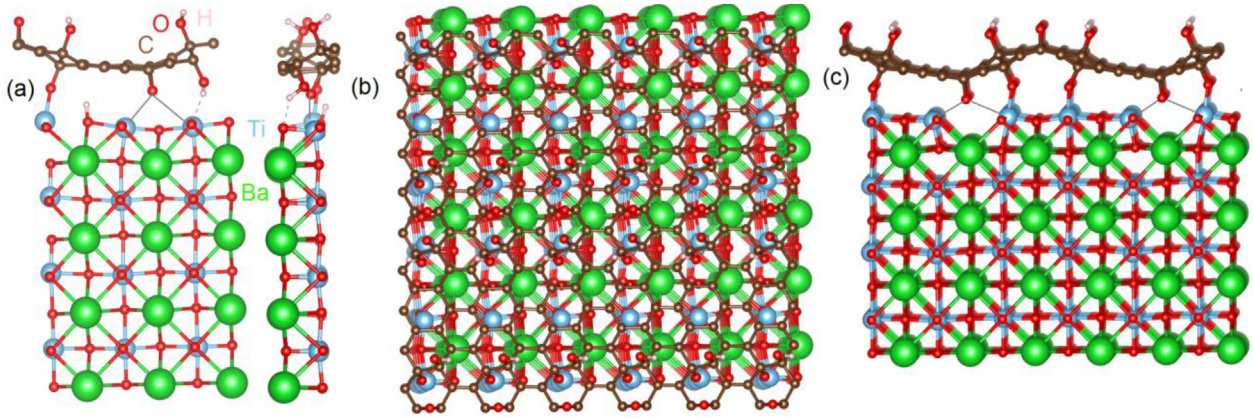

Fig. 4. Different side views of the optimized atomic structure of the supercell used for the modeling of the $BaTiO_3$/graphene oxide interface with smaller number of covalent bonds per surface unit (a) and top (b) and side (c) view of multiplied supercell used for the modeling of $BaTiO_3$/graphene oxide interface with larger number of covalent bonds per surface unit. Coordination bonds between epoxy group on graphene and titanium atoms are indicated by tiny lines.

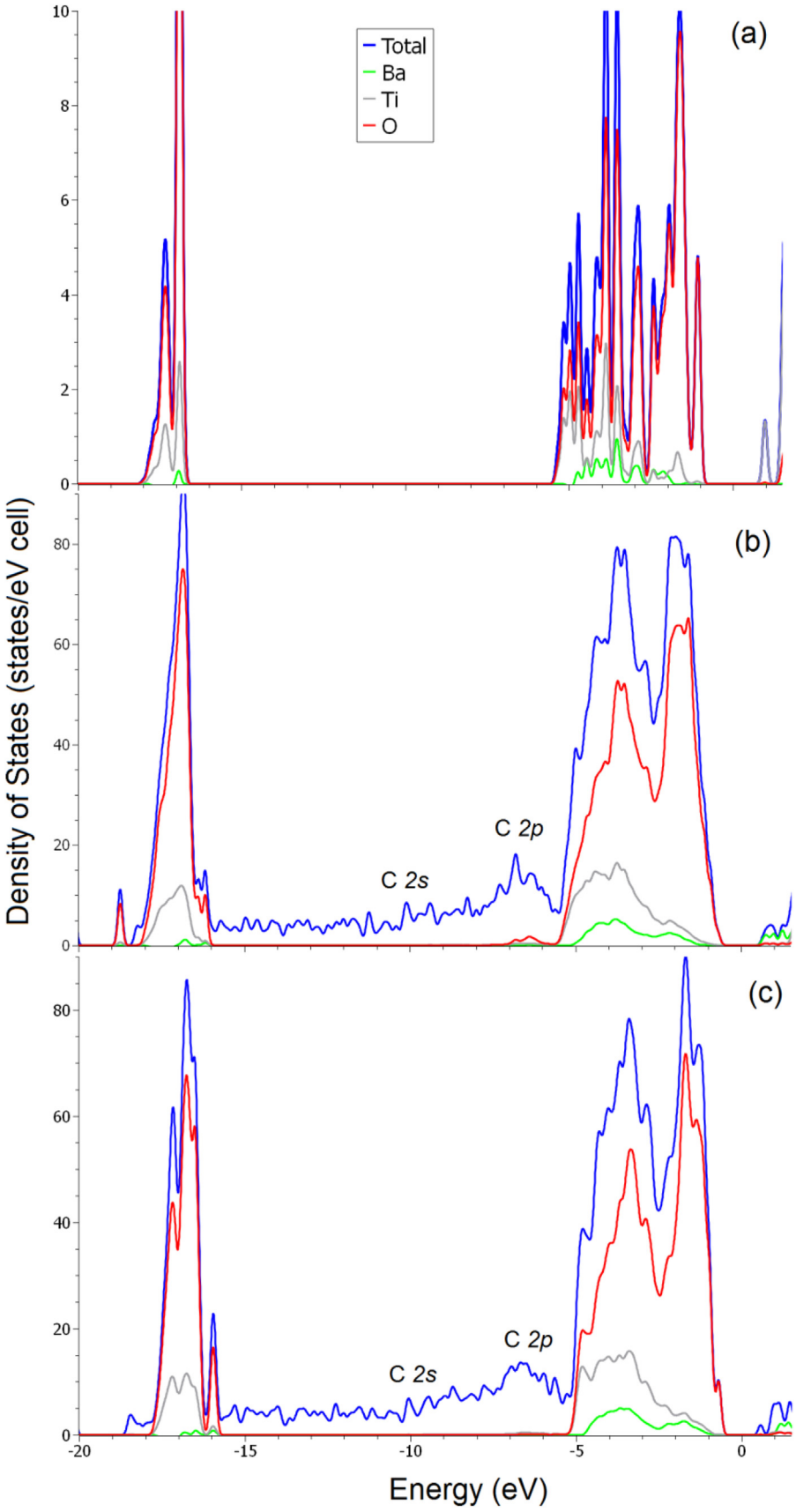

Fig. 5. Total and partial densities of states for bulk $BaTiO_3$ (a) and $BaTiO_3$/graphene interface with smaller (b) and larger (c) number of covalent bonds per surface unit. Note that on panel (b) and (c) the densities of states for the oxygen are provided only for the $BaTiO_3$ substrate. Fermi energy is set to zero.

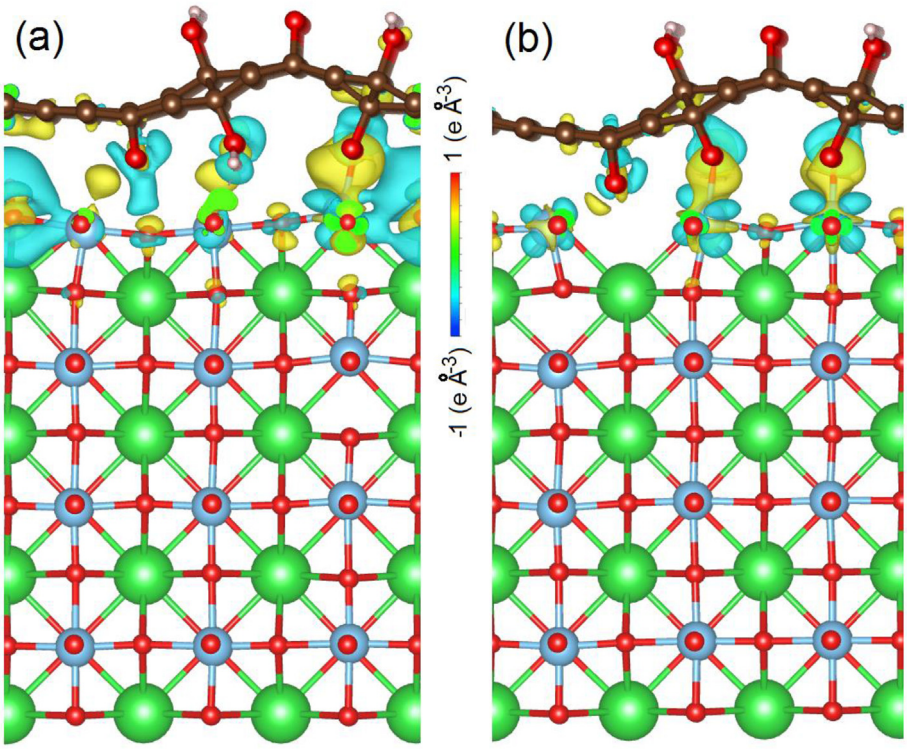

Fig. 6. Redistribution of charge densities after formation of one (a) and two (b) covalent bonds per supercell between $BaTiO_3$ and graphene oxide.

reveals the realistic graphene sheet over $BaTiO_3$ surface (Fig. 4b). For the modeling of graphene oxide we take our previously developed model [11,12] with a C:O ratio close to experimental (Fig. 2c).

Graphene oxide can be attached to $BaTiO_3$ substrate by different ways. The first one corresponds to covalent bonds when titanium atoms from the $BaTiO_3$ surface interact with the hydroxyl groups of graphene oxide. Hydrogen atoms from hydroxyl groups can interact with oxygen atoms of $BaTiO_3$ (Fig. 4a) or be removed as water molecules after formation of the pair of covalent bonds per supercell (Fig. 4c) . The second type of bonds is the coordination of titanium atoms by epoxy groups on graphene oxide (Fig. 4a,c). The next step of our calculations is the estimation of the enthalpy of formation of the studied interfaces. This value is defined as the difference between total energies of products and reactants. In the case shown on Fig. 4a the enthalpy of formation is −1.88 eV per Ti−O−C bond and in the case shown on Fig. 4c the value of the enthalpy is −0.60 eV per T-O-C bond. In both cases, the negative sign and rather large magnitude of the enthalpy evidence formation of robust Ti−O−C bonds. Smaller magnitudes in the second case are caused by the energy cost of the formation of oxygen defects in the $BaTiO_3$ surface. The cause of appearance of these defects is due to the formation of additional Ti−O−C to passivate dangling bonds. Taking into account the presence of oxygen vacancies in $BaTiO_3$ we have performed similar calculations for the presence single of an oxygen vacancy in the surface Ti−O layer. Calculated values are −3.16 and −1.11 eV per Ti−O−C bonds for the case of formation of one and two Ti−O−C bonds per supercell, respectively. Thus, the presence of oxygen vacancies increases the surface energy of $BaTiO_3$ making adsorption of graphene oxide more favorable.

The next step of our survey is the study of the influence of the formation of an interface with graphene oxide on the electronic structure of $BaTiO_3$. The results of the calculations (Fig. 5) demonstrate that formation of the interface leads to not only the appearance of C *2p* and C *2s* states in the total densities of states but also to a shift of the top of valence band of $BaTiO_3$ substrate towards the Fermi level. Thus, results of the theoretical modeling confirm the hypothesis discussed above that the shift of the top of the valence band in $BaTiO_3$/graphene oxide is related to the change of the electronic structure of the $BaTiO_3$ substrate. The changes in the electronic structure discussed above are related to a visible charge density redistribution in the surface and subsurface layers of $BaTiO_3$ (see Fig. 6). The calculated value of the electrons transferred from the barium titanate substrate to the graphene oxide is about 0.4 e^- per Ti−O−C bonds in both cases. Hence the shift of the top of the valence band towards the Fermi level caused by a p-doping of the $BaTiO_3$ substrate.

To prove the catalytic activity, we performed the modeling of the Volmer step of hydrogen evolution reaction in acidic and alkaline media. These processes are described by the following formulas:

$$H^+ + e^- \rightarrow *{-}H \quad (1)$$

$$H_2O + e^- \rightarrow *{-}H + OH^- \quad (2)$$

where * is the notation of the substrate. Based on our previous modeling of the catalytic properties of graphene oxide [12] we propose that the hydrogen atom should adsorb on the epoxy group with transformation of this group to hydroxyl group. The calculated free energies of these reactions are −0.48 eV/H and +1.65 eV/H. Both values are of the same order than recently reported theoretical values for the hydrogen evolution reaction over novel 2D materials [28]. Thus, we can propose $BaTiO_3$/graphene oxide as a prospective photo-catalyst due to the combination of a narrowed bandgap in $BaTiO_3$ core and a large number of active sites on the graphene shell.

4. Conclusions

Based on our XPS measurements and DFT calculations we can conclude that an interfacial interaction between graphene oxide and $BaTiO_3$ matrix with formation of Ti—O—C chemical bonds takes place in $BaTiO_3$/graphene composites, which means that in the given case graphene acts as an active filler. A similar effect with formation of Ti—O—C interfacial chemical bonds is observed in TiO_2/graphene composites [24]. The formation of Ti—O—C bonds in $BaTiO_3$/graphene composites not only improves the charge separation and electron transfer from $BaTiO_3$ to graphene but it also induces the reduction of the band gap of the synthesized nanocomposite which is favorable for the enhancement of the photocatalytic activity.

Declaration of competing interest

The authors declare that they have no known competing financial interests or personal relationships that could have appeared to influence the work reported in this paper.

CRediT authorship contribution statement

D.W. Boukhvalov: Investigation, Conceptualization, Writing - original draft. **I.S. Zhidkov:** Investigation, Formal analysis. **A.I. Kukharenko:** Investigation, Formal analysis. **S.O. Cholakh:** Data curation, Resources. **J.L. Menéndez:** Investigation, Funding acquisition, Methodology, Writing - review & editing. **L. Fernández-García:** Investigation. **E.Z. Kurmaev:** Conceptualization, Data curation, Writing - original draft.

Acknowledgements

XPS measurements are supported by Ministry of Science and Education of Russian Federation: Themes “Electron” № АААА-А18-118020190098-5 and the Government of the Russian Federation (Act 211, agreement No. 02.A03.21.0006).

References

[1] J.R.A.R. Bunsell, Fundamentals of Fiber Reinforced Composite Materials, vol. 398, CRC Press, London, 2005.
[2] S. Ariharan, A. Nisar, N. Balaji, et al., Carbon nanotubes stabilize high temperature phase and toughen Al2O3-based thermal barrier coatings, Compos. B Eng. 124 (2017) 76—87.
[3] S. Li, Z. Xie, Y. Zhang, et al., Enhanced toughness of zirconia ceramics with graphene platelets consolidated by spark plasma sintering, Int. J. Appl. Ceram. Technol. 14 (2017) 1062—1068.
[4] J.P. Fan, D.M. Zhuang, D.Q. Zhao, G. Zhang, M.S. Wu, F. Wei, Z.J. Fan, Toughening and reinforcing alumina matrix composite with single-wall carbon nanotubes, Appl. Phys. Lett. 89 (2006) 121910.
[5] G.D. Zhan, J.D. Kuntz, J.E. Garay, A.K. Mukherjee, Electrical properties of nanoceramics reinforced with ropes of single-walled carbon nanotubes, Appl. Phys. Lett. 83 (6) (2003) 1228—1230.
[6] H. Porwal, S. Grasso, M.J. Reece, Review of graphene—ceramic matrix composites, Adv. Appl. Ceramics 112 (2013) 443—454.
[7] Y.C. Fan, L.J. Wang, J.L. Li, J.Q. Li, S.K. Sun, F. Chen, L.D. Chen, W. Jiang, Preparation and electrical properties of graphene nanosheet/Al2O3 composites, Carbon 48 (2010) 1743—1749.
[8] T. He, J.L. Li, L.J. Wang, J.J. Zhu, W. Jiang, Preparation and consolidation of alumina/graphene composite powders, Mater. Trans. 50 (2009) 749—751.
[9] J. Liu, G. Tian, S. Qi, Z. Wu, D. Wu, Enhanced dielectric permittivity of a flexible three-phase polyimide—graphene—$BaTiO_3$ composite material, Mater. Lett. 124 (2014) 117—119.
[10] Y. Qing, Q. Wen F. Luo, W. Zhou, D. Zhu, Graphene nanosheets/$BaTiO_3$ ceramics as highly efficient electromagnetic interference shielding materials in the X-band, J. Mater. Chem. C 4 (2016) 371—375.
[11] I. Ahmad, M. Islam, N.H. Alharthi, H. Alawadhi, T. Subhani, K.S. Munir, S.I. Shah, F. Inam, Y. Zhu, Chemical and structural analyses of the graphene nanosheet/alumina ceramic interfacial region in rapidly consolidated ceramic nanocomposites, J. Compos. Mater. 52 (2017) 417—428.
[12] J.M. Soler, E. Artacho, J.D. Gale, A. Garsia, J. Junquera, P. Orejon, D. Sanchez-Portal, The SIESTA method for ab initio order-N materials simulation, J. Phys. Condens. Matter 14 (2002) 2745.
[13] D.W. Boukhvalov, M.I. Katsnelson, Modeling of graphite oxide, J. Am. Chem. Soc. 130 (2008) 10697—10701.
[14] D.W. Boukhvalov, D.R. Dreyer, C.W. Bielawski, Y.-W. Son, A computational investigation of the catalytic properties of graphene oxide: exploring mechanisms by using DFT methods, ChemCatChem 4 (2012) 1844—1849.
[15] J.P. Perdew, K. Burke, M. Ernzerhof, Generalized gradient approximation made simple, Phys. Rev. Lett. 77 (1996) 3865.
[16] M. Dion, H. Rydberg, H. Schröder, D.C. Langreth, B.I. Lundqvist, Van der Waals density functional for general geometries, Phys. Rev. Lett. 92 (2004), 246401.
[17] O.N. Troullier, J.L. Martins, Efficient pseudopotentials for plane-wave calculations, Phys. Rev. B 43 (1991) 1993.
[18] H.J. Monkhorst, J.D. Pack, Special points for Brillouin-zone integrations, Phys. Phys. Rev. B 13 (1976) 5188.
[19] C. Botas, P. Alvarez, C. Blanco, R. Santamaría, M. Granda, M.D. Gutierrez, et al., Critical temperatures in the synthesis of graphene-like materials by thermal exfoliation-reduction of graphite oxide, Carbon 52 (2013) 476.
[20] A.C. Ferrari, J.C. Meyer, V. Scardaci, C. Casiraghi, M. Lazzeri, F. Mauri, et al., Raman spectrum of graphene and graphene layers, Phys. Rev. Lett. 97 (2006) 187401.
[21] B. Liu, Y. Huang, Y. Wen, L. Du, W. Zeng, Y. Shi, F. Zhang, G. Zhu, X. Xu, Y. Wang, Highly dispersive {001} facets-exposed nanocrystalline TiO_2 on high quality graphene as a high performance photocatalyst, J. Mater. Chem. 22 (2012) 7484.
[22] Q. Zhang, N. Bao, X. Wang, X. Hu, X. Miao, M. Chaker, D. Ma, Advanced fabrication of chemically bonded graphene/TiO_2 continuous fibers with enhanced broadband photocatalytic properties and involved mechanisms exploration, Sci. Rep. 6 (2016) 38066.
[23] D. Zhao, G. Sheng, C. Chen, X. Wang, Enhanced photocatalytic degradation of methylene blue under visible irradiation on graphene@TiO_2 dyade structure, Appl. Catal. B Environ. 111 (2012) 303—308.
[24] G. Sobon, J. Sotor, J. Jagiello, R. Kozinski, M. Zdrojek, M. Holdynski, P. Paletko, J. Boguslawski, L. Lipinska, K.M. Abramski, Graphene Oxide vs. Reduced Graphene Oxide as saturable absorbers for Er-doped passively mode-locked fiber laser, Optic Express 20 (2012) 19463—19473.
[25] D. Ehre, H. Cohen, V. Lyahovitskaya, I. Lubomirsky, X-ray photoelectron spectroscopy of amorphous and quasiamorphous phases of $BaTiO_3$ and $SrTiO_3$, Phys. Rev. B 77 (2008), 181406.
[28] G. D'Olimpio, C. Guo, C.-N. Kuo, R. Edla, C.S. Lue, L. Ottaviano, P. Torelli, L. Wang, D.W. Boukhvalov, A. Politano, $PdTe_2$ transition-metal dichalcogenide: chemical reactivity, thermal stability and device implementation, Adv. Funct. Mater. 30 (2020), 1906556.